# Interpenetrating Metal−Metalloporphyrin Framework for Selective CO_2 Uptake and Chemical Transformation of CO_2

Wen-Yang Gao,[†] Chen-Yen Tsai,[†,‡] Lukasz Wojtas,[†] Timmy Thiounn,[†] Chu-Chieh Lin,[‡] and Shengqian Ma*,[†]

[†]Department of Chemistry, University of South Florida, 4202 East Fowler Avenue, Tampa, Florida 33620, United States
[‡]Department of Chemistry, National Chung Hsing University, Taichung 402, Taiwan

⑤ *Supporting Information*

ABSTRACT: Herein we report a robust primitive cubic (pcu)-topology metal−metalloporphyrin framework (MMPF), MMPF-18, which was constructed from a ubiquitous secondary building unit of a tetranuclear zinc cluster, $Zn_4(\mu_4\text{-}O)(-COO)_6$, and a linear organic linker of 5,15-bis(4-carboxyphenyl)porphyrin (H_2bcpp). The strong $\pi-\pi$ stacking from porphyrins and the lengthy H_2bcpp ligand affords a 4-fold-interpenetrating network along with reduced void spaces and confined narrow channels. Thereby, MMPF-18 presents segmented pores and high-density metalloporphyrin centers for selective CO_2 uptake over CH_4 and size-selective chemical transformation of CO_2 with epoxides forming cyclic carbonates under ambient conditions.
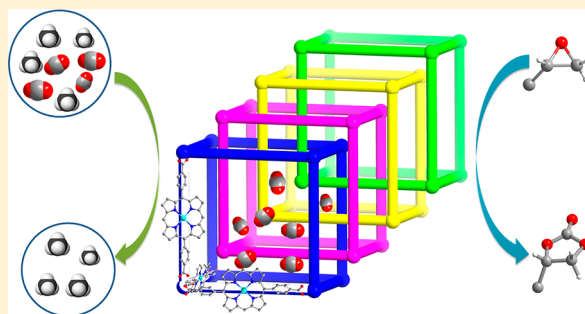
INTRODUCTION

Carbon dioxide (CO_2), accumulating in the atmosphere at an alarming rate, is deemed as the major greenhouse gas causing global warming over the past several decades. In order to reduce greenhouse emissions, it has become imperative to develop applicable CO_2 capture and sequestration (CCS) technologies.[1] Beyond the well-studied CCS using sorbent materials,[2] CO_2 chemical transformation forming value-added industrial products turns into an alternative yet sustainable means, given that CO_2 represents an abundant, nontoxic, and inexpensive C1 building block.[3] In particular, the synthesis of cyclic carbonates from CO_2 and epoxides is of great promise because of high atom efficiency, and the generated carbonates can be broadly utilized as starting materials for electrolytes, polycarbonates, and aprotic polar solvents. A variety of homogeneous catalysts were thus exploited to promote the efficient synthesis of cyclic carbonates from CO_2 and epoxides via cycloaddition reactions, including salen-type complexes[4] and metalloporphyrins.[5] Among them, zinc (Zn) and magnesium (Mg) are the most common metal species included in porphyrin cores as highly efficient Lewis acid catalysts for cycloaddition reactions. In contrast with homogeneous systems requiring rigorous separation and purification of the products, heterogeneous systems exhibit simple separation of catalysts from the products with the possibility of recycling or reusing the catalysts. Therefore, it is highly desired to heterogenize well-developed Zn-based porphyrin catalysts for CO_2 chemical transformation with epoxides to form cyclic carbonates.

Over the last 2 decades, metal−organic frameworks (MOFs) have been advanced as a new class of functional porous materials that are built from metal-ion nodes (or secondary building units, SBUs) connected by organic linkers through coordination bonds.[6] Considering their crystalline periodic networks with tunable pore sizes and functionalities, MOFs have deeply revolutionized the areas of materials science and adsorbent development. As an important subclass of MOFs, metal−metalloporphyrin frameworks (MMPFs) have been attracting escalating interest because of their promising utilization for gas adsorption/separation, catalysis, light harvesting, etc.[7]

Bearing all of the above in mind, a promising heterogeneous catalyst containing Zn-based porphyrins for CO_2 chemical transformation can be rationalized by employing a custom-designed porphyrin as the organic linker to build a Zn-based framework in which the porphyrin core can be in situ metalated with Zn^{II}. Under guidance of this strategy, a robust MMPF, MMPF-18, was constructed from a linear organic linker of 5,15-bis(4-carboxyphenyl)porphyrin (H_2bcpp) and a ubiquitous SBU of $Zn_4(\mu_4\text{-}O)(-COO)_6$, of which the porphyrin core was in situ metalated by Zn^{II}. Moreover, strong $\pi-\pi$ stacking from porphyrins and the lengthy H_2bcpp ligand affords a 4-fold-interpenetrating primitive cubic (pcu)-topology network along with reduced void spaces and confined narrow channels. MMPF-18 thereby presents segmented pores and high-density metalloporphyrin centers for selective CO_2 uptake over CH_4 and highly efficient size-selective chemical transformation of

CO_2 with epoxides forming cyclic carbonates under ambient conditions (under 1 atm of pressure at room temperature). Our studies also prove that interpenetration can be an effective means to boost the stability of MOF structures as well as to render pore sizes and functionalities for size-selective guest separation and heterogeneous catalysis.[8]

■ EXPERIMENTAL SECTION

The dark-colored cubic-shaped crystals of MMPF-18 were collected by mixing H_2bcpp with $Zn(NO_3)_2 \cdot 6H_2O$ under solvothermal reaction conditions. Single-crystal X-ray diffraction studies reveal that MMPF-18 crystallizes in the rhombohedral space group $R\bar{3}c$ accompanied by the empirical formula $Zn_4(\mu_4\text{-}O)(Zn\text{-}bcpp)_3$. As shown in Figure 1a, a
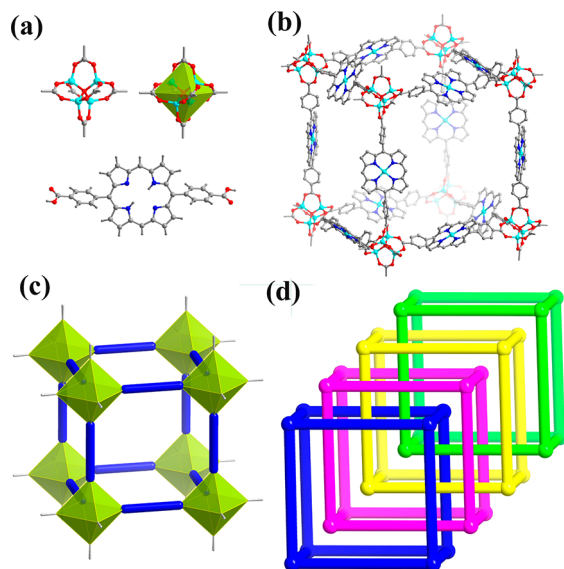

Figure 1. (a) Ubiquitous SBU of $Zn_4(\mu_4\text{-}O)(-COO)_6$ and the linear porphyrin linker of H_2bcpp used in the construction of MMPF-18. (b) Resultant pcu-topology MMPF-18 structure containing the in situ metalated Zn-based porphyrin. (c) Simplified noninterpenetrated pcu-topology network. (d) Resultant 4-fold-interpenetrating network of MMPF-18.

ubiquitous SBU of $Zn_4(\mu_4\text{-}O)(-COO)_6$ is observed in MMPF-18, serving as a 6-connected node. Each linear linker of bcpp bridges two adjacent SBUs via carboxylate groups coordinating with Zn^{II} ions, thus affording a pcu-topology network (Figure 1b,c), similarly to the prototypal MOF-5 built from the SBUs of $Zn_4(\mu_4\text{-}O)(-COO)_6$ and a linear linker of terephthalic acid.[9] However, because of strong $\pi-\pi$ stacking from porphyrins and the lengthy H_2bcpp ligand, a 4-fold-interpenetrating network is thus generated (illustrated in Figure 1d), whereas a reduced void space may create confined narrow pores/channels, only permitting accessibility of size/dimension-suitable guest molecules. More importantly, solvothermal reaction enables the bcpp porphyrin ligands to be in situ metalated with Zn^{II} ions. Thus, MMPF-18 is obtained as a 4-fold-interpenetrating pcu-topology network featuring segmented pores and high-density Zn-based porphyrin centers, which render its potential for selective CO_2 uptake and size-selective chemical fixation of CO_2 with epoxides and other catalysis studies.

Powder X-ray diffraction analysis was employed to verify the phase purity of MMPF-18. The results show that the diffraction patterns of the fresh MMPF-18 sample are in good agreement with the calculated ones (Figure S1). Thermogravimetric analysis (TGA) on the fresh sample of MMPF-18 (Figure S2) indicates a continuous weight loss of ~22% from 25 to 300 °C due to the elimination of guest solvent molecules in the channels. The plot is followed by a relatively short plateau from 300 to 390 °C. Then MMPF-18 starts to fall into

decomposition from 390 to 495 °C with another weight loss of ~14%. The TGA results indicate that, after removal of guest molecules, MMPF-18 exhibits relatively high thermal stability up to 390 °C with certain structural robustness.

Gas adsorption measurements were conducted on the MMPF-18 sample preactivated by solvent exchange and high vacuum (more details in the Supporting Information), in order to study its permanent porosity and robustness. As shown in Figure 2a, the nitrogen (N_2)
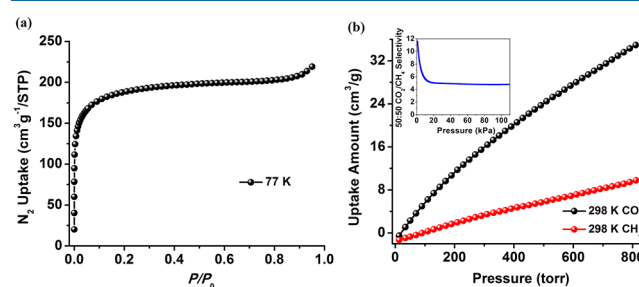

Figure 2. (a) N_2 adsorption isotherm of MMPF-18 at 77 K. (b) CO_2 and CH_4 adsorption isotherms of MMPF-18 at 298 K and (inset) IAST selectivity for 50:50 CO_2/CH_4 binary mixtures at 298 K.

adsorption isotherm at 77 K demonstrates an uptake capacity of ~220 $cm^3 \ g^{-1}$ at 1 atm of pressure, which belongs to a typical type I adsorption isotherm of microporous materials. On the basis of the N_2 adsorption isotherm at 77 K, MMPF-18 owns a Brunauer−Emmett−Teller surface area of 700 $m^2 \ g^{-1}$ ($P/P_0 = 0.0001-0.1$) along with a Langmuir surface area of 824 $m^2 \ g^{-1}$ ($P/P_0 = 0.0001-0.1$). Pore-size distribution analysis (Figure S3) using the density functional theory model illustrates that the pore sizes of MMPF-18 are predominantly distributed at the sizes of ~7 and ~12 Å, which are consistent with the widths of the channels observed in the crystal structure.
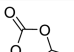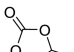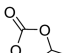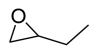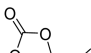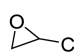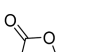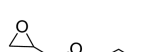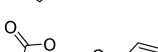
■ RESULTS AND DISCUSSION

Considering the pores segmented by interpenetration and the resultant high-density metalloporphyrin centers in MMPF-18, we initially evaluated their functionalities for CO_2 uptake performances prior to exploring their catalytic performance. As illustrated in Figure S4, MMPF-18 demonstrates moderate CO_2 uptake capacities of 60.0 $cm^3 \ g^{-1}$ (11.8 wt %) at 273 K and 33.6 $cm^3 \ g^{-1}$ (6.6 wt %) at 298 K under 1 atm of pressure. On the basis of CO_2 adsorption isotherms at 273 and 298 K, the isosteric heats of adsorption (Q_{st}) of CO_2 for MMPF-18 were then determined by the virial method (Figure S5). As shown in F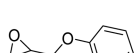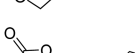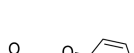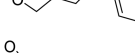igure S6, MMPF-18 exhibits a constant Q_{st} of ~23 kJ mol^{-1} at all loadings, which can be presumably ascribed to the high density of open metalloporphyrin sites on the limited exposed surface of MMPF-18. Furthermore, to predict the CO_2 separation performance over CH_4 at 298 K, the selectivity for 50:50 CO_2/CH_4 binary mixtures was estimated up to 1 atm from the single-component gas-adsorption isotherms (Figure 2b) utilizing ideal adsorbed solution theory (IAST).[10] As shown in Figure 2b (inset), MMPF-18 exhibits certain selectivity of CO_2 over CH_4 at 298 K, particularly at the low loading range, which can be tentatively attributed to the confined pore sizes resulting from interpenetration and the open metal sites saturated along with the increasing loading.

Considering the high density of accessible metalloporphyrin centers in the nanoscopic channels and previous studies on using Zn-based porphyrins as efficient homogeneous catalysts for CO_2 chemical fixation, we decided to investigate the performance of MMPF-18 as a Lewis acid catalyst for cycloaddition reactions from CO_2 and epoxides forming cyclic

carbonates under ambient conditions (at room temperature under 1 atm of pressure).[11] MMPF-18 displays great catalytic efficiency for CO_2 coupled with propylene oxide forming propylene carbonate under ambient conditions with a yield of 96.97% (Table 1, entry 1) over 48 h. MMPF-18 dramatically

Table 1. Cycloaddition Reactions Promoted by Different Catalysts from Different Substituted Epoxides and CO_2

Entry	Epoxides	Products	Yield (%)
1[a]			96.97
2[b]			49.20
3[c]			98.20
4[a]			96.63
5[a]			99.00
6[a]			99.60
7[a]			33.25
8[c]			44.20

[a]Reaction conditions: epoxide (10.0 mmol), n-Bu$_4$NBr (232.0 mg), and MMPF-18 (17.6 mg, 0.25 mol % based on metalloporphyrin core), under 1 atm of CO_2 at room temperature for 48 h. The yield was monitored by ^{1}H NMR. [b]The same conditions but loaded with HKUST-1 (0.125 mol % per dicopper-paddlewheel SBUs). [c]The same conditions but loaded with Zn-TPP (0.25 mol % based on a metalloporphyrin core).

exceeds the benchmark MOF of HKUST-1 with 49.20% yield (Table 1, entry 2) under similar reaction conditions, which features Lewis acid sites from a copper-paddlewheel SBU. Meanwhile, the catalytic efficiency of MMPF-18 is comparable to that of a homogeneous zinc tetraphenylporphyrin (Zn-TPP) catalyst (Table 1, entry 3). The remarkable catalytic efficiency of MMPF-18 for CO_2 chemical transformation should be attributed to not only strong Lewis acidity from Zn-based porphyrins, as observed in homogeneous systems, but also accessible porosities facilitating substrate mass transfer. In order to generalize the results of this study, we systematically evaluated the catalytic activity of MMPF-18 in CO_2 chemical transformation with different functional-group-substituted epoxides under ambient conditions. MMPF-18 also exhibits high catalytic efficiency for cycloaddition reactions of butylene oxide, epichlorohydrin, and allyl glycidyl ether using CO_2 to form butylene carbonate (Table 1, entry 4), chloroethylene carbonate (Table 1, entry 5), and allyl glycidyl carbonate (Table 1, entry 6) with yields of 96.63%, 99.00%, and 99.60%, respectively, over 48 h. Furthermore, an impressive decrease in the yield of cyclic carbonate was observed with an increase of the molecular size of the epoxide substrate, as illuminated by the 33.25% yield of phenyl glycidyl carbonate (Table 1, entry 7)

from phenyl glycidyl ether. Compared to a homogeneous Zn-TPP catalyst with a 44.20% yield of phenyl glycidyl carbonate (Table 1, entry 8), the lower yield of MMPF-18 could be ascribed to not only the intrinsic activity of the substrate but also the limited diffusion of the large substrate into the narrow channels of MMPF-18, hence displaying size-selective catalysis.[12]

CONCLUSIONS

In summary, a robust pcu-topology MMPF, MMPF-18, was built from a linear free-base porphyrin that connects the prototypal SBU of $Zn_4(\mu_4\text{-O})(-COO)_6$. Strong $\pi-\pi$ stacking from porphyrins and the lengthy H_2bcpp ligand offers a 4-fold-interpenetrating network along with reduced void spaces and confined narrow channels. Meanwhile, the porphyrin cores were in situ metalated under solvothermal reaction conditions. Thus, MMPF-18 presents the limited pore size and high-density metalloporphyrin centers enabled by interpenetration for selective CO_2 uptake over CH_4 and size-selective chemical transformation of CO_2 with epoxides into cyclic carbonates under ambient conditions, although its chemical stability needs to be boosted in terms of long-term application.[13] It can be further anticipated that interpenetration can be considered an effective means to not only enhance the stability of MOF structures but also render pore sizes and functionalities for size-selective separation and heterogeneous catalysis.

ASSOCIATED CONTENT

Ⓢ Supporting Information

The Supporting Information is available free of charge on the ACS Publications website at DOI: 10.1021/acs.inorgchem.6b00937.

Details of experiments and characterizations (PDF)

X-ray crystallographic data in CIF format (CIF)

AUTHOR INFORMATION

Corresponding Author

*E-mail: sqma@usf.edu.

Notes

The authors declare no competing financial interest.

ACKNOWLEDGMENTS

REFERENCES

(1) (a) Chu, S. Science **2009**, 325, 1599. (b) Li, J.-R.; Ma, Y.; McCarthy, M. C.; Sculley, J.; Yu, J.; Jeong, H.-K.; Balbuena, P. B.; Zhou, H.-C. Coord. Chem. Rev. **2011**, 255, 1791−1823.

(2) (a) Liu, J.; Thallapally, P. K.; McGrail, B. P.; Brown, D. R.; Liu, J. Chem. Soc. Rev. **2012**, 41, 2308−2322. (b) Sumida, K.; Rogow, D. L.; Mason, J. A.; McDonald, T. M.; Bloch, E. D.; Herm, Z. R.; Bae, T.-H.; Long, J. R. Chem. Rev. **2012**, 112, 724−781.

(3) (a) Lanzafame, P.; Centi, G.; Perathoner, S. Chem. Soc. Rev. **2014**, 43, 7562−7580. (b) Gao, W.-Y.; Wu, H.; Leng, K.; Sun, Y.; Ma, S. Angew. Chem., Int. Ed. **2016**, 55, 5472−5476.

(4) (a) North, M.; Pasquale, R. Angew. Chem., Int. Ed. **2009**, 48, 2946−2948. (b) Luo, R.; Zhou, X.; Chen, S.; Li, Y.; Zhou, L.; Ji, H. Green Chem. **2014**, 16, 1496−1506. (c) Wang, Y.; Qin, Y.; Wang, X.; Wang, F. Catal. Sci. Technol. **2014**, 4, 3964−3972.

(5) (a) Ema, T.; Miyazaki, Y.; Shimonishi, J.; Maeda, C.; Hasegawa, J.-y. *J. Am. Chem. Soc.* **2014**, *136*, 15270−15279. (b) Maeda, C.; Taniguchi, T.; Ogawa, K.; Ema, T. *Angew. Chem., Int. Ed.* **2015**, *54*, 134−138. (c) Maeda, C.; Shimonishi, J.; Miyazaki, R.; Hasegawa, J.-y.; Ema, T. *Chem. - Eur. J.* **2016**, *22*, 6556−6563.

(6) (a) Zhou, H.-C.; Kitagawa, S. *Chem. Soc. Rev.* **2014**, *43*, 5415−5418. (b) Li, B.; Chrzanowski, M.; Zhang, Y.; Ma, S. *Coord. Chem. Rev.* **2016**, *307*, 106−129.

(7) (a) Gao, W.-Y.; Chrzanowski, M.; Ma, S. *Chem. Soc. Rev.* **2014**, *43*, 5841−5866. (b) Zhao, M.; Ou, S.; Wu, C.-D. *Acc. Chem. Res.* **2014**, *47*, 1199−1207. (c) Suslick, K. S.; Bhyrappa, P.; Chou, J. H.; Kosal, M. E.; Nakagaki, S.; Smithenry, D. W.; Wilson, S. R. *Acc. Chem. Res.* **2005**, *38*, 283−291.

(8) (a) Li, H.; Eddaoudi, M.; O'Keeffe, M.; Yaghi, O. M. *Nature* **1999**, *402*, 276−279. (b) Smithenry, D. W.; Wilson, S. R.; Suslick, K. S. *Inorg. Chem.* **2003**, *42*, 7719−7721.

(9) (a) Jiang, H.-L.; Makal, T. A.; Zhou, H.-C. *Coord. Chem. Rev.* **2013**, *257*, 2232−2249. (b) Ma, S.; Sun, D.; Ambrogio, M.; Fillinger, J. A.; Parkin, S.; Zhou, H.-C. *J. Am. Chem. Soc.* **2007**, *129*, 1858−1859.

(10) (a) Myers, A. L.; Prausnitz, J. M. *AIChE J.* **1965**, *11*, 121−127. (b) Bae, Y. S.; Mulfort, K. L.; Frost, H.; Ryan, P.; Punnathanam, S.; Broadbelt, L. J.; Hupp, J. T.; Snurr, R. Q. *Langmuir* **2008**, *24*, 8592−8598.

(11) (a) Gao, W.-Y.; Chen, Y.; Niu, Y.; Williams, K.; Cash, L.; Perez, P. J.; Wojtas, L.; Cai, J.; Chen, Y.-S.; Ma, S. *Angew. Chem., Int. Ed.* **2014**, *53*, 2615−2619. (b) Gao, W.-Y.; Wojtas, L.; Ma, S. *Chem. Commun.* **2014**, *50*, 5316−5318. (c) Beyzavi, M. H.; Klet, R. C.; Tussupbayev, S.; Borycz, J.; Vermeulen, N. A.; Cramer, C. J.; Stoddart, J. F.; Hupp, J. T.; Farha, O. K. *J. Am. Chem. Soc.* **2014**, *136*, 15861−15864.

(12) (a) Horike, S.; Dinca, M.; Tamaki, K.; Long, J. R. *J. Am. Chem. Soc.* **2008**, *130*, 5854−5855. (b) Liu, J.; Chen, L.; Cui, H.; Zhang, J.; Zhang, L.; Su, C.-Y. *Chem. Soc. Rev.* **2014**, *43*, 6011−6061.

(13) Fernandez, C. A.; Thallapally, P. K.; Liu, J.; Peden, C. H. F. *Cryst. Growth Des.* **2010**, *10*, 4118−4122.